

## Note: Control parameter dependence of fluctuations near jamming

Harukuni Ikeda<sup>1, a)</sup>

*Department of Physics, Gakushuin University, 1-5-1 Mejiro, Toshima-ku, Tokyo 171-8588, Japan*

(Dated: 25 January 2023)

In this work, we report the control parameter dependence of the fluctuations near the jamming transition point. We show that the fluctuations do not diverge in pressure control, while it diverges in packing fraction control.

We consider purely repulsive harmonic discs in a two-dimensional  $L \times L$  box with periodic boundary conditions at zero temperature<sup>1</sup>:

$$V_N = \sum_{i < j}^{1, N} \frac{h_{ij}^2}{2} \theta(-h_{ij}), \quad h_{ij} = |\mathbf{r}_i - \mathbf{r}_j| - R_i - R_j, \quad (1)$$

where  $N$  denotes the number of particles,  $\mathbf{r}_i = (x_i, y_i)$  denotes the position, and  $R_i$  denotes the radius. To avoid crystallization, we consider a 50 : 50 binary mixture of large  $R_L = 0.7$  and small  $R_s = 0.5$  particles. The value of  $V_N$  separates the jammed and unjammed phases: when the packing fraction  $\varphi = N\pi(R_s^2 + R_L^2)/(2L^2)$  is smaller than the jamming transition point  $\varphi_J$ , one observes  $V_N = 0$  after the energy minimization, while, when  $\varphi > \varphi_J$ ,  $V_N$  has a finite value. For the energy minimization, we use the fast inertial relaxation engine (FIRE)<sup>2</sup>. We terminate the energy minimization when  $\sum_{i=1}^N (\partial_{\mathbf{r}_i} V_N)^2 / N < 10^{-25}$ . In our numerical simulation, we define  $\varphi_J$  at which the energy barely has a finite value  $V_N/N \in (10^{-16}, 2 \times 10^{-16})$  after the energy minimization. We generate the configurations above  $\varphi_J$  in two ways, as described below.

*a. Packing fraction control* We use  $\varepsilon = \varphi - \varphi_J$  as a control parameter. Following O' Hern *et al.*, we first generate the configuration at  $\varphi_J$  by combining compression and decompression: we compress the system when  $V_N < 10^{-16}$  and decompress when  $V_N > 10^{-16}$ , see Ref<sup>1</sup> for details. After every compression/decompression, we minimize the energy by using the FIRE algorithm<sup>2</sup>. We terminate the process when  $V_N/N \in (10^{-16}, 2 \times 10^{-16})$ . After obtaining a configuration at  $\varphi_J$ , we re-compress as the amount of  $\varepsilon = \varphi - \varphi_J$  to obtain a configuration above jamming. As reported in Ref.<sup>3</sup>, some samples unjam after the compression (compression unjamming). We throw out such samples.

*b. Pressure control* The pressure  $p$  is used as the control parameter. For this purpose, we repeat the compression and decompression until the system's pressure reaches the target pressure. In this case, the jamming transition point corresponds to  $p = 0$ .

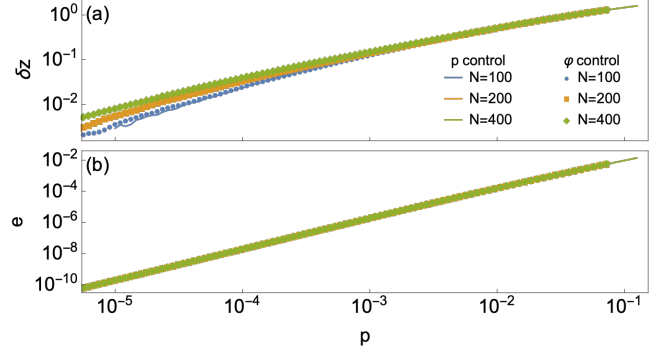


FIG. 1. Fluctuations of physical quantities. Solid lines and markers denote data for  $p$  and  $\varphi$  control, respectively. For comparison, results for  $\varphi$  control are plotted as a function of the average  $p$  at each  $\varphi$ . (a) Contract number. (b) Energy per particle  $e = V_N/N$ .

For each  $\varepsilon$  and  $p$ , we prepare  $M = 1000$  independent samples and calculate the mean and variance of physical quantities. We only use the data for  $p \gg 10^{-6}$  so that the force balance tolerance and energy tolerance do not affect the results.

We first discuss the behaviors of the average quantities. A commonly observed quantity to characterize the jamming transition is the number of contacts per particle  $z$ . At  $\varphi_J$ ,  $z$  converges to  $z_J = 2d - 2d/N + 2/N$ , if one removes rattlers that have less than three contacts<sup>4</sup>. Hereafter we remove the rattlers when calculating  $z$ . Another commonly used quantity is the energy per particle  $e = V_N/N$ . In Fig. 1, we plot the average values of the excess contact number  $\delta z = z - z_J$  and  $e$ . It can be seen that the average values do not depend on the control parameters.

Next, we discuss the fluctuations. To see how large the fluctuation is compared to the mean value, we observe the following quantities:

$$\chi_z \equiv N \frac{\text{Var}(z)}{\text{Ave}(z)^2}, \quad \chi_e \equiv N \frac{\text{Var}(e)}{\text{Ave}(e)^2}, \quad (2)$$

where Var and Ave respectively denote the variance and average for the  $M$  samples. The factor  $N$  guarantees that  $\chi_{z,e}$  converges to a finite value in the thermodynamic limit  $N \rightarrow \infty$ <sup>5</sup>. In Fig. 2, we plot the numerical results of  $\chi_z$  and  $\chi_e$ . In  $p$  control, the  $N$  dependence of  $\chi_z$  only appears very near the jamming transition point,  $p \lesssim 10^{-4}$ . The finite size effects in this region are examined in detail in Ref.<sup>5</sup>. We do not observe any significant  $N$  dependence for  $\chi_e$ . On the contrary, in  $\varphi$  control, both  $\chi_z$  and  $\chi_e$  significantly increase with  $N$  in the intermediate region ( $10^{-3} \lesssim p \lesssim 10^{-2}$  for  $\chi_z$ , and  $10^{-5} \lesssim p \lesssim 10^{-2}$

<sup>a)</sup>Electronic mail: harukuni.ikeda@gakushuin.ac.jp

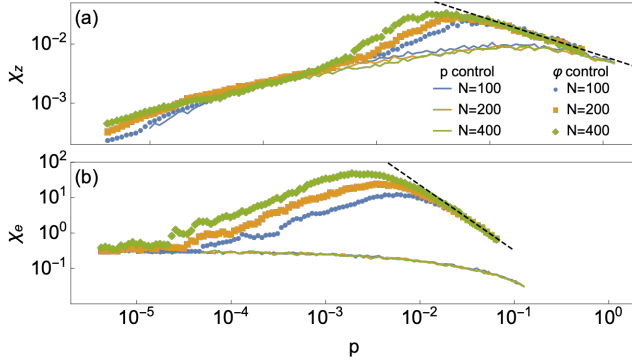


FIG. 2. Fluctuations of physical quantities. Solid lines and markers denote data for  $p$  and  $\varphi$  control, respectively. Black dashed lines denote power-law fit. For comparison, results for  $\varphi$  control are plotted as a function of the average  $p$  at each  $\varphi$ . (a) Fluctuation of the contact number. (b) Fluctuation of energy.

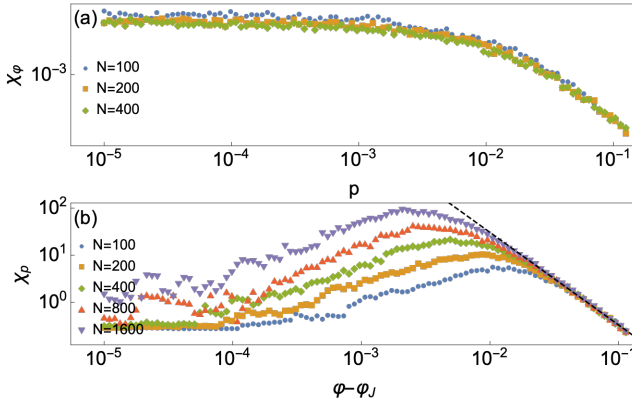


FIG. 3. Fluctuations of (a)  $\varphi$  in  $p$  control and (b)  $p$  in  $\varphi$  control. Markers denote numerical results, while the dashed line shows the power-law fit.

for  $\chi_e$ ). In the intermediate  $\varphi$  region,  $\chi_{z,e}$  is well fitted with the power-law function:

$$\chi_{z,e} = A_{z,e} p^{-\beta_{z,e}}, \quad (3)$$

where  $\beta_z = 0.62$  and  $\beta_e = 1.85$ , see black dashed lines in Fig. 2. The power-law region increases with  $N$ , and in the thermodynamic limit, the fluctuations are expected to diverge at the transition point. In Fig. 3, we plot the fluctuation of  $\varphi$ ,  $\chi_\varphi \equiv N\text{Var}(\varphi)/\text{Ave}(\varphi)^2$ , in  $p$  control and the fluctuation of  $p$ ,  $\chi_p \equiv N\text{Var}(p)/\text{Ave}(p)^2$ , in  $\varphi$  control. We found that  $\chi_\varphi$  remains finite, while  $\chi_p$  exhibits a power-law divergence  $\chi_p \sim (\varphi - \varphi_J)^{-\beta_p}$  with  $\beta_p = 1.97$ , see the dashed line in Fig. 3.

Finally, we propose a phenomenological model to explain the divergence of the physical quantities in  $\varphi$  control. Fig. 3 (a) and a previous research<sup>1</sup> show that the variance of  $\varphi$  remains finite at  $\varphi_J$ . Also,  $p \propto \varphi - \varphi_J$  near  $\varphi_J$ . Therefore,  $p$  and  $\varphi$  have the following linear relation near  $\varphi_J$ :  $\varphi = \varphi_J + Ap + \xi$ , where  $\xi$  is a random variable of zero mean and variance  $\xi^2 = \Delta/N^6$ , and  $A$  and  $\Delta$  are

constants. Then,  $p$  can be expressed as a function of  $\delta\varphi$ :

$$p = A^{-1}(\delta\varphi - \xi), \quad (4)$$

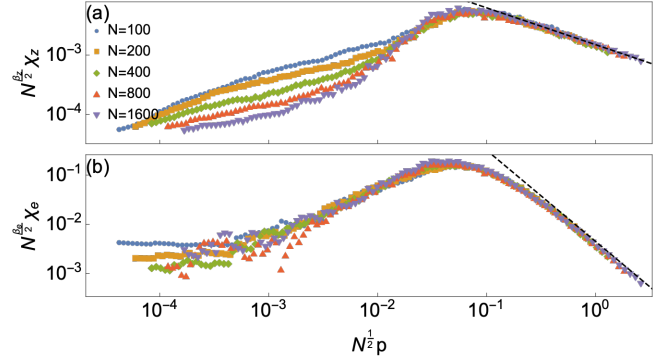


FIG. 4. Scaling plots for (a)  $\chi_z$  and (b)  $\chi_e$  in  $\varphi$  control. Markers denote numerical results, while the dashed lines denote power-law fit  $A_{z,e} p^{\beta_{z,e}}$ .

with  $\delta\varphi = \varphi - \varphi_J$ . It is straightforward to show  $\chi_p \sim \delta\varphi^{-\beta_p^{th}} \sim p^{-\beta_p^{th}}$  with  $\beta_p^{th} = 2$ , which is close to the numerical result  $\beta_p = 1.97$ . Since the energy is a quadratic function of  $p$ ,  $e \sim p^2 = A^{-2}(\delta\varphi^2 - 2\delta\varphi\xi + \dots)$ , leading to  $\chi_e \sim p^{-\beta_e^{th}}$  with  $\beta_e^{th} = 2$ . Again, this is close to the numerical result  $\beta_e = 1.85$ . The contact number exhibits the square-root singularity  $z - z_J \sim p^{1/2} = A^{-1/2}(\delta\varphi^{1/2} - \xi\delta\varphi^{-1/2}/2 + \dots)$ , leading to  $\chi_z \sim p^{-\beta_z^{th}}$  with  $\beta_z^{th} = 1/2$ , which is slightly underestimated but close to the numerical result  $\beta_z = 0.62$ . The above mean-field like argument may no-longer hold when the fluctuation of the pressure  $A^{-1}\xi$  becomes larger than the mean-value  $A^{-1}\delta\varphi$  in Eq. (4), which defines the characteristic pressure  $p \sim \delta\varphi \sim \xi \sim O(N^{-1/2})$ . This consideration suggests the following scaling form:

$$\chi_{z,e} = N^{\frac{\beta_{z,e}}{2}} f_{z,e}(N^{1/2}p), \quad (5)$$

where  $f_{z,e}(x)$  denotes the scaling function such that  $f_{z,e}(x) \sim x^{-\beta_{z,e}}$  for  $x \ll 1$ . In Fig. 4, we confirmed the above scaling ansatz using the data shown in Fig. 2 and data for larger  $N$  in  $\varphi$  control.

## ACKNOWLEDGMENTS

We thank A. Ikeda, P. Urbani, and F. Zamponi for useful comments. This work was supported by KAKENHI 21K20355.

## DATA AVAILABILITY

The data that support the findings of this study are available from the corresponding author upon reasonable request.

<sup>1</sup>C. S. O'Hern, L. E. Silbert, A. J. Liu, and S. R. Nagel, Phys. Rev. E **68**, 011306 (2003).

<sup>2</sup>E. Bitzek, P. Koskinen, F. Gähler, M. Moseler, and P. Gumbsch, Phys. Rev. Lett. **97**, 170201 (2006).

<sup>3</sup>K. VanderWerf, A. Boromand, M. D. Shattuck, and C. S. O'Hern, Phys. Rev. Lett. **124**, 038004 (2020).

<sup>4</sup>C. P. Goodrich, A. J. Liu, and S. R. Nagel, Phys. Rev. Lett. **109**, 095704 (2012).

<sup>5</sup>D. Hexner, P. Urbani, and F. Zamponi, Phys. Rev. Lett. **123**, 068003 (2019).

<sup>6</sup>F. Zamponi (private communication).